



Controllability of cupric particle synthesis by linear alcohol chain number as additive and pH control in cupric acetate solution using X-ray radiolysis

Akinobu Yamaguchi,^{a*} Ikuo Okada,^b Ikuya Sakurai,^b Hirokazu Izumi,^c Mari Ishihara,^c Takao Fukuoka,^a Satoru Suzuki,^a Kelvin Elphick,^d Edward Jackson,^d Atsufumi Hirohata^d and Yuichi Utsumi^a

Received 3 May 2019

Accepted 24 July 2019

Edited by Y. Amemiya, University of Tokyo, Japan

Keywords: X-ray radiolysis; cupric particle; alkyl alcohol; pH control; three-dimensional additive manufacturing.

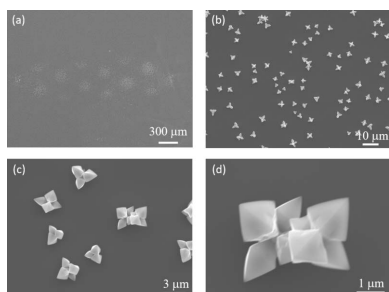
^aLaboratory of Advanced Science and Technology for Industry, University of Hyogo, 3-1-2 Koto, Kamigori, Hyogo 678-1205, Japan, ^bSynchrotron Radiation Research Center, Nagoya University, Furo-cho, Chikusa-ku, Nagoya, Aichi 464-8603, Japan, ^cHyogo Prefectural Institute of Technology, 3-1-12 Yukihiro, Suma, Kobe 654-0037, Japan, and ^dDepartment of Electronic Engineering, University of York, Heslington, York YO10 5DD, UK.

*Correspondence e-mail: yamaguti@lasti.u-hyogo.ac.jp

Synthesis and immobilization of caltrop cupric particles onto a Si substrate using X-ray radiolysis directly from a liquid solution of $\text{Cu}(\text{COOCH}_3)_2$ is demonstrated. Caltrop cupric oxide particles are formed in the X-ray radiolysis of aqueous solutions of $\text{Cu}(\text{COOCH}_3)_2$, which also contain methanol, ethanol, 2-propanol or 1-propanol as $\cdot\text{OH}$ scavenger. The blade lengths of the caltrop particles are dependent on the alcohol chain length. In particular, it was found that an alkyl alcohol whose chain length is longer than four is unable to synthesize any particles in aqueous solutions of $\text{Cu}(\text{COOCH}_3)_2$ in X-ray radiolysis. These results are attributed to the alkyl alcohol chain length influencing the rate of reaction of radicals and determines the solvable ratio of its alcohol into water. In addition, it was found that the synthesized particle geometric structure and composition can also be controlled by the pH of the aqueous solution in the X-ray radiolysis. This study may open a door to understanding and investigating a novel photochemical reaction route induced under X-ray irradiation. The development of the X-ray radiolysis process enables us to achieve the rapid and easy process of synthesis and immobilization of higher-order nano/microstructure consisting of various materials.

1. Introduction

Nano/microscale materials have attracted much attention because of their potential applicability ranging from fundamental science to engineering applications. They are expected to exhibit remarkable optical, electrical, magnetic and mechanical properties (Kreibig & Vollmer, 1995; Le Ru & Etchegoin, 2009; Lu *et al.*, 2009; Cushing *et al.*, 2004). For example, surface-enhanced Raman scattering (SERS) can be a highly sensitive detection tool for a small amount of substrate (Le Ru & Etchegoin, 2009; Albrecht & Creighton, 1977; Haynes *et al.*, 2005; Nie & Emory, 1997). Chemical synthesis of inorganic materials with conventional and novel morphologies has been developed for crucial applications such as catalysts, medicine, electronics, ceramics, cosmetics and bio-sensing using SERS. Recently, many structured nanoparticles and nanostructures, such as nanorods, nanowires, nanoribbons, nanobelts, nano-flowers and caltrop particles, have been synthesized by various techniques (Lu *et al.*, 2009; Cushing *et al.*, 2004; Gedanken, 2004; Nagata *et al.*, 1992; Wagner &



Köhler, 2005; Suslick *et al.*, 1991; Bang & Suslick, 2010; Caruso *et al.*, 2002; Mori *et al.*, 2004; Tu & Liu, 2000; Yamamoto *et al.*, 2004; Okitsu *et al.*, 2001; Frens, 1972; Frens, 1973; Athawale *et al.*, 2005; Tsuji *et al.*, 2005; Takami *et al.*, 1999; Hashimoto *et al.*, 2011; Bae *et al.*, 2002; Fievet *et al.*, 1989; Figlarz *et al.*, 1985; Wiley *et al.*, 2004; Kvítek *et al.*, 2008; Hara *et al.*, 2014; Ma *et al.*, 2000; Rosenberg *et al.*, 1998; Borse *et al.*, 2004a,b 2004; Lee *et al.*, 2003; Remita *et al.*, 2005, 2007; Dey, 2005, 2011; Bárta *et al.*, 2010; Yamaguchi *et al.*, 2015, 2016a,b, 2017; Bharti *et al.*, 2016; Zhang *et al.*, 2014; Zhang *et al.*, 2005; Su *et al.*, 2014; Poizot *et al.*, 2000; Volanti *et al.*, 2008; Kim *et al.*, 2010; Park *et al.*, 2012; Clay & Cohen, 1998; Long *et al.*, 2009; Dar *et al.*, 2009; Yeh *et al.*, 1999; Radi *et al.*, 2010; Izaki *et al.*, 2007; Fleisch & Mains, 1982; Tamaki *et al.*, 1998; Zaman *et al.*, 2011, 2012; Shao *et al.*, 2007; Zhang *et al.*, 2006; Lisiecki & Pileni, 1993; Brookshier *et al.*, 1999).

In particular, the synthesis of cupric oxide particles has attracted considerable attention due to their fundamental importance and potential future applications (see references above). For example, cupric oxides (*e.g.* Cu_2O and CuO) are used in the anodes of lithium ion cells, combined with ZnO in heterostructure solar-cell panels and incorporated into gas sensors because they are p-type semiconductor materials with narrow band gap energy (Izaki *et al.*, 2007). Clay & Cohen (1998) synthesized CuO nanoclusters within films of diblock copolymers. Volanti *et al.* (2008) demonstrated a CuO flower-shaped nanostructure processed by a hydrothermal microwave oven technique. In addition, the caltrop cupric oxide micro/nanoparticles including both Cu_2O and CuO have been directly synthesized from $\text{Cu}(\text{COOCH}_3)_2$ aqueous solution by X-ray radiolysis within additive ethanol (Yamaguchi *et al.*, 2017).

Here, we have noticed that the additive ethanol plays a significant role in the reduction and synthesis of caltrop cupric oxide particles directly from solution by X-ray radiolysis (Yamaguchi *et al.*, 2016a,b, 2017). The reduction effect induced by the additive alcohol has been reported in sonochemistry (Gedanken, 2004; Nagata *et al.*, 1992; Suslick *et al.*, 1991; Bang & Suslick, 2010; Caruso *et al.*, 2002; Mori *et al.*, 2004), hydrothermal microwave synthesis (Tsuji *et al.*, 2005; Volanti *et al.*, 2008; Dar *et al.*, 2009) and photochemical reactions using UV radiation (Takami *et al.*, 1999; Hashimoto *et al.*, 2011; Bae *et al.*, 2002; Bárta *et al.*, 2010; Long *et al.*, 2009; Dar *et al.*, 2009; Fleisch & Mains, 1982). The reduction effect of alcohol should represent an important direction for the synthesis of nanomaterials using X-ray radiolysis (Remita *et al.*, 2007; Yamaguchi *et al.*, 2015, 2016a,b, 2017; Bharti *et al.*, 2016) or γ -ray radiolysis (Dey, 2005, 2011; Bárta *et al.*, 2010). We should investigate the controllability of cupric particle synthesis by linear alcohol chain number as additive and pH control in liquid solution using the X-ray radiolysis process to understand the mechanism of particle nucleation, ripening and aggregation. In this paper, we report the controlled synthesis and immobilization of caltrop cupric oxide particles by X-ray irradiation using synchrotron radiation, and their material properties.

Table 1

Summary of solutions prepared for the X-ray irradiation experiments.

Solution number	$\text{Cu}(\text{COOCH}_3)_2$	Type and amount of additive
#1	200 μL	Not applicable
#2: R-1	200 μL	Methanol, 10 μL
#3: R-2	200 μL	Ethanol, 10 μL
#4: R-3	200 μL	1-Propanol, 10 μL
#5: R-4	200 μL	1-Butanol, 10 μL
#6: R-5	200 μL	1-Pentanol, 10 μL
#7: R-6	200 μL	1-Hexanol, 10 μL
#8: R-7	200 μL	1-Heptanol, 10 μL
#9: R-8	200 μL	1-Octanol, 10 μL
#10: R-9	200 μL	1-Nonanol, 10 μL
#11: R-10	200 μL	1-Decanol, 10 μL
#12: R-2'	200 μL	2-Propanol, 10 μL
#13	200 μL	Acetone, 10 μL
#14	200 μL	Acetic acid, 10 μL

2. Experimental setup

Synchrotron-radiation-induced X-ray radiolysis experiments were performed using beamline BL8S2 at the Aichi Synchrotron Radiation Center, Aichi Science and Technology Foundation, Japan. Based on our previous X-ray radiolysis experiment setup (Yamaguchi *et al.*, 2015, 2016a,b, 2017), a 100 ml aliquot of 0.37 mol L^{-1} (M) $\text{Cu}(\text{COOCH}_3)_2$ (purchased from FUJIFILM Wako Pure Chemical Corporation, Wako 1st Grade) was prepared by diluting the stock solution before the following experiments. Here, ultra-pure water prepared by a Milli-Q system (Merck KGaA) was used for sample preparation.

We conducted two experiments to reveal the alkyl alcohol chain number dependence and the pH dependence of X-ray radiolysis-induced particle synthesis. At first, to study the chain length dependence, we performed X-ray irradiation of the cupric acetate, $0.37 M$ $\text{Cu}(\text{COOCH}_3)_2$ solution, including alkyl alcohol from methanol (R-1) to 1-decanol (R-10), and 2-propanol (R-2'). All alkyl alcohols and 2-propanol were prepared as Wako 1st Grade from FUJIFILM Wako Pure Chemical Corporation. We siphoned off 200 μL of the stock solution, $0.37 M$ $\text{Cu}(\text{COOCH}_3)_2$, into a microtube, and added 10 μL of each alcohol listed in Table 1 to obtain a mixed solution. We prepared 12 kinds of solution to investigate the alcohol chain length dependence of the X-ray radiolysis-induced particle synthesis. In addition, we prepared two kinds of solution using either acetone or acetic acid. The compositions of the prepared solution are summarized in Table 1.

Next, we carried out an experiment to investigate the pH dependence of X-ray radiolysis; guaranteed reagent ammonia (NH_3) or hydrochloric acid (HCl), purchased from FUJIFILM Wako Pure Chemical Corporation, was added to control the pH of the $0.37 M$ $\text{Cu}(\text{COOCH}_3)_2$ solution with methanol. The pH of the original stock solution of $0.37 M$ $\text{Cu}(\text{COOCH}_3)_2$ was about 6. Accordingly, solutions with pH of 1, 3, 6, 7, 9 and 11 were prepared.

We siphoned off an 18 μL aliquot of each mixed solution and poured it into the apparatus for the liquid irradiation. A silicon substrate (size: 10 mm \times 10 mm; thickness: 525 μm ;

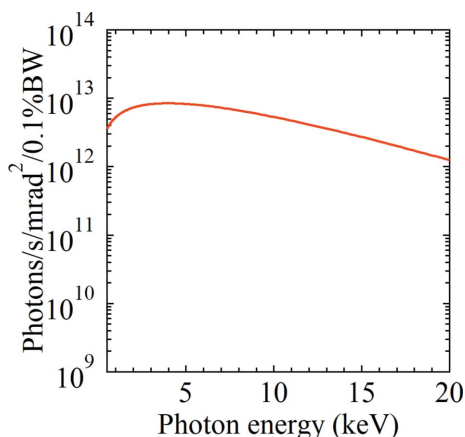


Figure 1
X-ray spectrum obtained at BL8S1 of Aichi Synchrotron Radiation Center.

Matsuzaki Seisakusho Co. Ltd) was dipped into the solution in the apparatus. Then, the specimen was exposed to polychromatic X-ray irradiation for 5 min. The corresponding X-ray spectrum is shown in Fig. 1. The irradiation experiment was performed at room temperature. After the irradiation, the specimen temperature was anticipated to be raised by about 15°C. After 5 min of X-ray irradiation, some particles and their aggregates were deposited and immobilized on the silicon substrate. The silicon substrates were taken out from the specimen and gently washed with ionized water to remove residual materials.

Then, scanning electron microscopy (SEM) (FE-SEM, Jeol, JSM-7001F) with energy-dispersive X-ray spectroscopy (EDX) was performed. Raman spectra of the synthesized particles were also measured using a micro-Raman spectrometer (JASCO, NRS-5100). The excitation source had a wavelength of 532 nm (a green laser) and power of 3.2 mW, which was magnified using a 100× field lens. The laser spot diameter was measured to be about 1 μm. All the characterization experiments were performed at room temperature.

3. Results and discussion

After X-ray irradiation and cleaning by ultra-pure water, SEM observation on all the irradiated substrates was performed. After irradiation, we also checked the SiN membrane windows to confirm whether or not any particles were synthesized and immobilized onto the membrane. As a result, 5 min of X-ray irradiation experiments to reveal the chain length dependence of additive alcohol show that no particles were nucleated when a silicon substrate was immersed in aqueous Cu(COOCH₃)₂ solution including no additive and the following alkyl alcohols: 1-butanol (R-4), 1-pentanol (R-5), 1-hexanol (R-6), 1-heptanol (R-7), 1-octanol (R-8), 1-nonanol (R-9) and 1-decanol (R-10). We found that the synthesis behavior with adding the alcohol induced by X-ray radiolysis drastically controls the chain length of the alkyl alcohol. The threshold chain length is found to be associated with the solubility character of alcohols. There is no limit on the amount of methanol (R-1), ethanol (R-2) and propanol

Table 2
Summary of solubilities of alcohols in water.

Formula	Name	Solubility in water (g/100 g)
CH ₃ OH	Methanol	Infinitely soluble
CH ₃ CH ₂ OH	Ethanol	Infinitely soluble
CH ₃ (CH ₂) ₂ OH	Propanol	Infinitely soluble
CH ₃ (CH ₂) ₃ OH	Butanol	7–13 at about 300 K (pp. 32–36†)
CH ₃ (CH ₂) ₄ OH	Pentanol	1.8–3.1 at about 300 K (pp. 162–167†)
CH ₃ (CH ₂) ₅ OH	Hexanol	~0.6 at about 300 K (pp. 263–268†)
CH ₃ (CH ₂) ₆ OH	Heptanol	0.13–0.3 at about 300 K (pp. 329–333†)
CH ₃ (CH ₂) ₇ OH	Octanol	~0.058 at about 300 K (pp. 364–368†)
CH ₃ (CH ₂) ₈ OH	Nonanol	~0.013 at about 300 K (pp. 392–396†)
CH ₃ (CH ₂) ₉ OH	Decanol	0.0032–0.005 at about 300 K (pp. 402–406†)

† The data are based on the data of Barton (1984).

(R-3) that can dissolve in a given quantity of water, while the solubility in water is limited by the fact that a hydrocarbon chain becomes longer than that of propanol (Barton, 1984). This solubility is considered to be a key factor with respect to the synthesis of particles induced by X-ray radiolysis, as summarized in Table 2.

Further, to investigate the redox properties, we confirmed that no particles were nucleated on a silicon substrate immersed in aqueous Cu(COOCH₃)₂ solution using acetone or acetic acid during the X-ray radiolysis. These results indicate that carboxylic acid and ketone are not appropriate reducing agents because C=O coupling is too strong to provide an electron or radical into the solution (Yates & Shinozaki, 1993). In the following, we focus on cases where synthesis and immobilization of particles occur on the silicon substrate.

Figs. 2 and 3 show typical SEM images and EDX analysis, observed and measured after 5 min of X-ray irradiation onto the Cu(COOCH₃)₂ solutions with methanol (R-1). As shown in Fig. 2, we found that caltrop-like microscale particles were

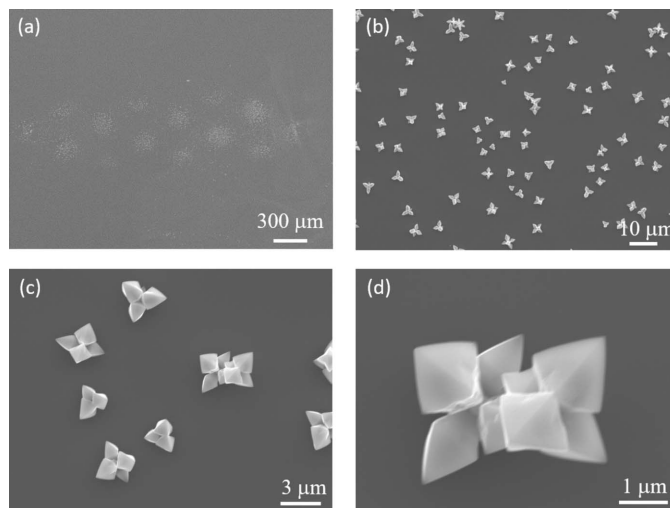


Figure 2
(a) SEM image of a Cu(COOCH₃)₂ solution with methanol (R-1) after X-ray irradiation for 5 min. (b) Magnified SEM image of caltrop cupric oxide particles nucleated from the mixed solution under X-ray irradiation. (c, d) High-resolution SEM images of the nucleated particles.

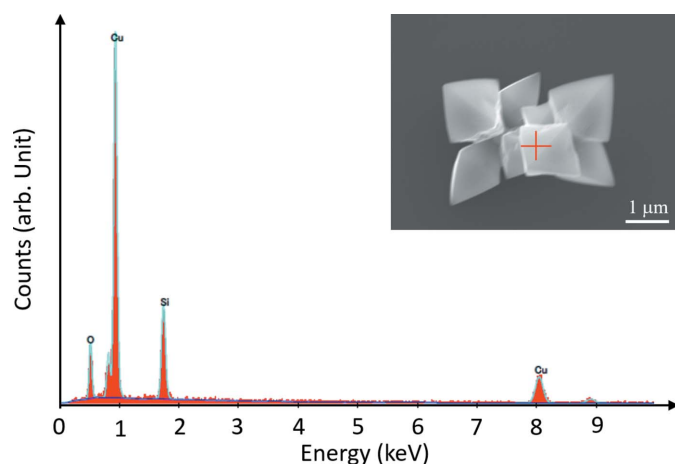


Figure 3
EDX spectrum measured from the position indicated by the red cross in the inset. The inset SEM image corresponds to the SEM image in Fig. 1(d).

deposited onto the silicon substrate. The EDX analysis in Fig. 3 reveals that the particles consisted of cupric oxide. SEM images of particles synthesized from the solutions with ethanol (R-2), 2-propanol (R-2') and 1-propanol (R-3) are displayed in Figs. 4, 5 and 6, respectively. A comparison of the SEM images shown in Figs. 4–6 indicates that the morphologies of the synthesized particles are dependent on the types of alcohol. The particle shapes synthesized from the solution with methanol and 1-propanol look very similar and are different from those from the solution with ethanol and 2-propanol. However, the comparison of the EDX analysis indicates that the constituent element of these particles synthesized by X-ray radiolysis with respective additive alcohols are almost the same. These individual EDX results are not shown here, because the EDX spectra are almost identical to Fig. 3. At the present stage, it is difficult to distinguish the

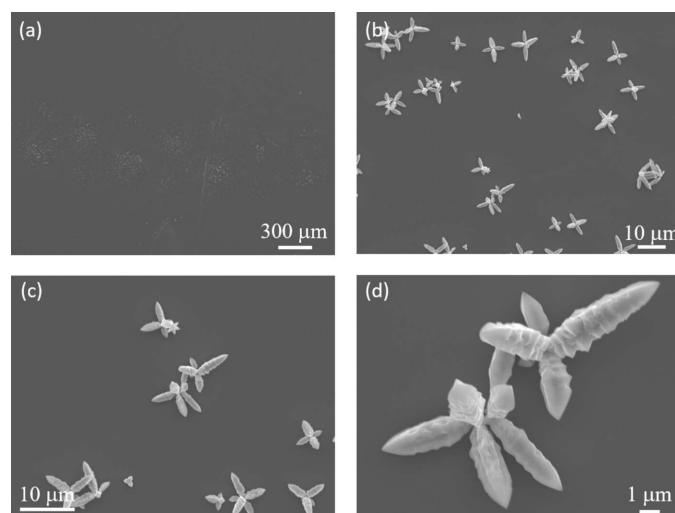


Figure 4
(a) SEM image of a $\text{Cu}(\text{COOCH}_3)_2$ solution with ethanol (R-2) after X-ray irradiation for 5 min. (b) Magnified SEM image of caltrop cupric oxide particles nucleated from the mixed solution under X-ray irradiation. (c, d) High-resolution SEM images of the nucleated particles.

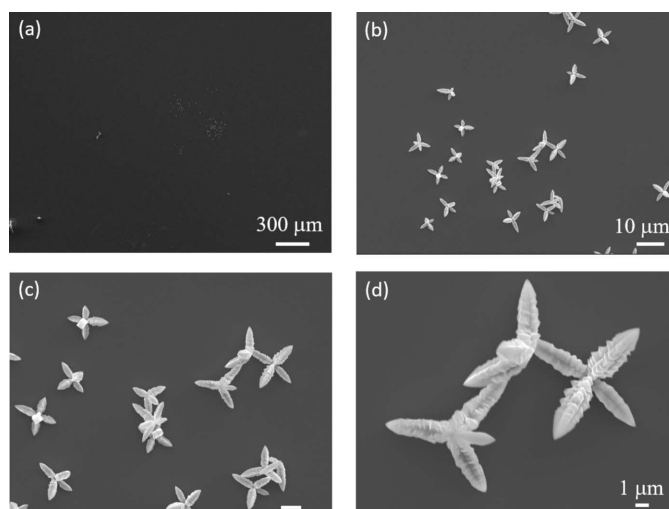


Figure 5
(a) SEM image of a $\text{Cu}(\text{COOCH}_3)_2$ solution with 2-propanol (R-2') after X-ray irradiation for 5 min. (b) Magnified SEM image of caltrop cupric oxide particles nucleated from the mixed solution under X-ray irradiation. (c, d) High-resolution SEM images of the nucleated particles.

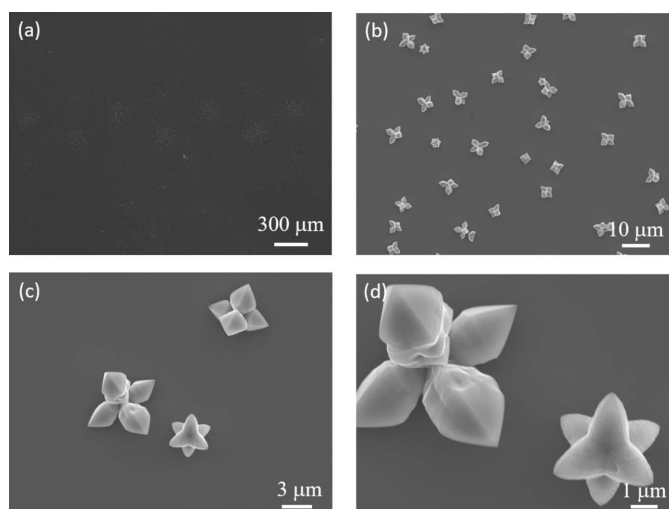


Figure 6
(a) SEM image of a $\text{Cu}(\text{COOCH}_3)_2$ solution with 1-propanol (R-3) after X-ray irradiation for 5 min. (b) Magnified SEM image of caltrop cupric oxide particles nucleated from the mixed solution under X-ray irradiation. (c, d) High-resolution SEM images of the nucleated particles.

compositions in the individual particles from the EDX analysis. Meticulously examining the EDX spectrum in Fig. 3, a split spectrum or spectrum consisting of several peaks around 0.9 keV is obtained for the peak derived from the Cu *L*-shell. The energies of characteristic X-rays of Cu are known as follows: 8.979 (*K* β), 8.040 (*K* α), 8.904 (*K* β), 0.933 (*L*III β), 0.953 (*L*II β), 1.100 (*L*I β) and 0.930 (*L* α) (Goldstein *et al.*, 2003). The characteristics are dependent on the selection rule and electron state modulated by the coupling and valence in the particles. This issue will be discussed later, again by showing the pH dependency of particle generation by X-ray radiolysis. The results are attributed to the competition between the particle nucleation and growth induced by the

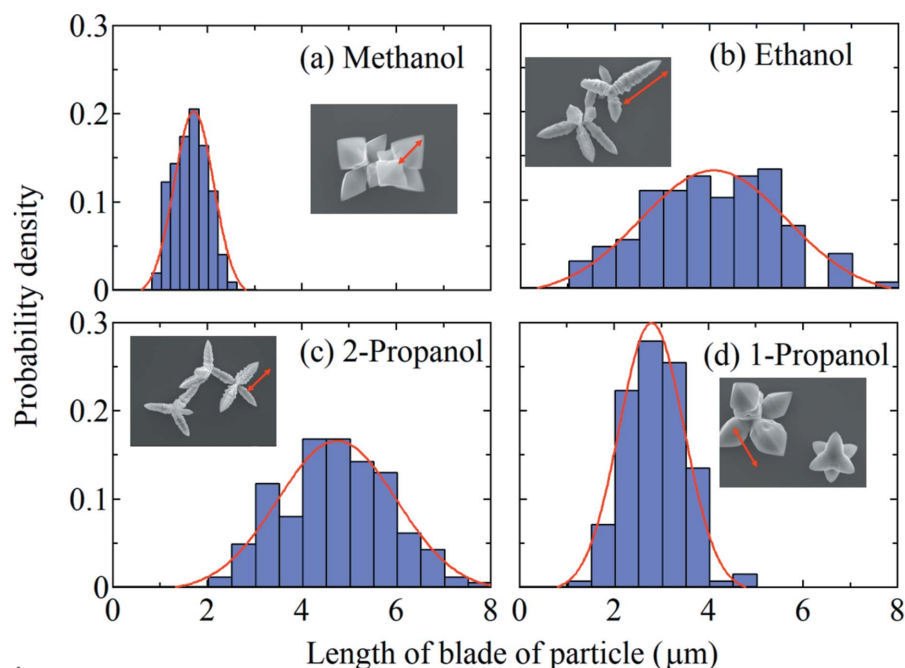


Figure 7
Probability densities of the blade length of particles synthesized by $\text{Cu}(\text{COOCH}_3)_2$ mixed with (a) methanol (R-1), (b) ethanol (R-2), (c) 2-propanol (R-2') and (d) 1-propanol (R-3), respectively. The insets show the definition of the blade length of the particles. The red fitting curves are Gaussian distributions.

effective reaction rate, which is dependent on the formation of radicals, scavenge rate and redox rate (Weiss, 1944, 1946; Miller, 1950; Samuel & Magee, 1953; Henglein, 2000; Johnsen *et al.*, 1969; Buxton *et al.*, 1988; Ervens *et al.*, 2003).

Now, we compare the size of the respective particles. To simplify the estimation of the synthesized particle size, we measure the blade length of the caltrop particles. The probability densities of the length of the particles synthesized by X-ray radiolysis with the additive (a) methanol (R-1), (b) ethanol (R-2), (c) 2-propanol (R-2') and (d) 1-propanol (R-3) are plotted as a function of blade length in Figs. 7(a), 7(b), 7(c) and 7(d), respectively. We imaged the particles immobilized onto the silicon substrate by SEM as displayed in Figs. 2, 4, 5 and 6, respectively. Blade numbers 194, 125, 125 and 160 were measured from the SEM images in the parent populations of Figs. 7(a), 7(b), 7(c) and 7(d), respectively. The blade length of particles gives an indication of the reactive characteristics. A higher ratio of the activity to reduce metallic ions or grow particles provides a longer blade length. The result shown in Fig. 8 indicates that the order of the average blade length in descending order is found to be [1] 2-propanol (R-2'), [2] ethanol (R-2), [3] 1-propanol (R-3) and [4] methanol (R-1). The average blade length for the case (R-1) is almost half that of cases (R-2) and (R-2'). Here, two aspects need to be considered with respect to 2-propanol (R-2'). First, that (R-2') of 2-propanol is defined as an ethanol-like chain, of which the basic chain is the same but is connected to two CH_3 . Second, that the two CH_3 functional groups of 2-propanol are so small that its polarity is similar to methanol rather than ethanol. The tertiary carbon atom of 2-propanol is the strongest for the radicalization. Here, we adopt the scheme that

simply aligns the chain length in order. We found that the length of the particle blade increases with the chain length for those below (R-2'), while the opposite behavior is shown for (R-3). The result is attributed to the presence of the strongest radicalizing tertiary carbon atom in 2-propanol. We also found that the alcohols with longer chain length than the chain length of (R-4) cannot synthesize any particles. According to Suslick *et al.* (1991), Bang & Suslick (2010), Caruso *et al.* (2002) and Mori *et al.* (2004), the particle size is inversely proportional to the alcohol concentration and the alkyl chain length. They argued that this is intimately related to the fact that alcohols absorbed on the surface of metal nuclei can limit the growth rate and can also stabilize particles of a smaller size, typically a few micrometres, to prevent further growth in sonochemical experiments. In sonochemical experiments, the volume where active cavitating bubbles appears and the number of cavitating bubbles

dominates the reaction process because a sufficient amount of alcohol is absorbed at the bubble interface to scavenge the maximum number of radicals produced by collapsing bubbles. It can be seen that our experimental results show a different trend for the results obtained in the sonochemical experiments. According to Caruso *et al.* (2002), the reduction process $\text{Au}(\text{III}) \rightarrow \text{Au}(0)$ in a gold particle using AuCl_4^- solution with additive alcohol by γ -ray radiolysis is partly catalytic, as significantly less than three electrons from reducing radicals are required to achieve the reduction. It may be expected that the alcohol type may influence the reduction rate, as the total amount absorbed onto the particle surface is limited to achieve the suitable reaction and to obtain stability through a

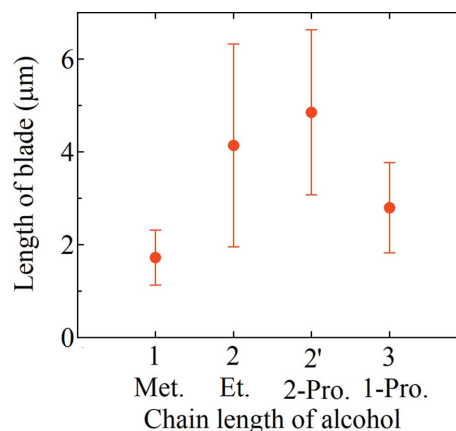
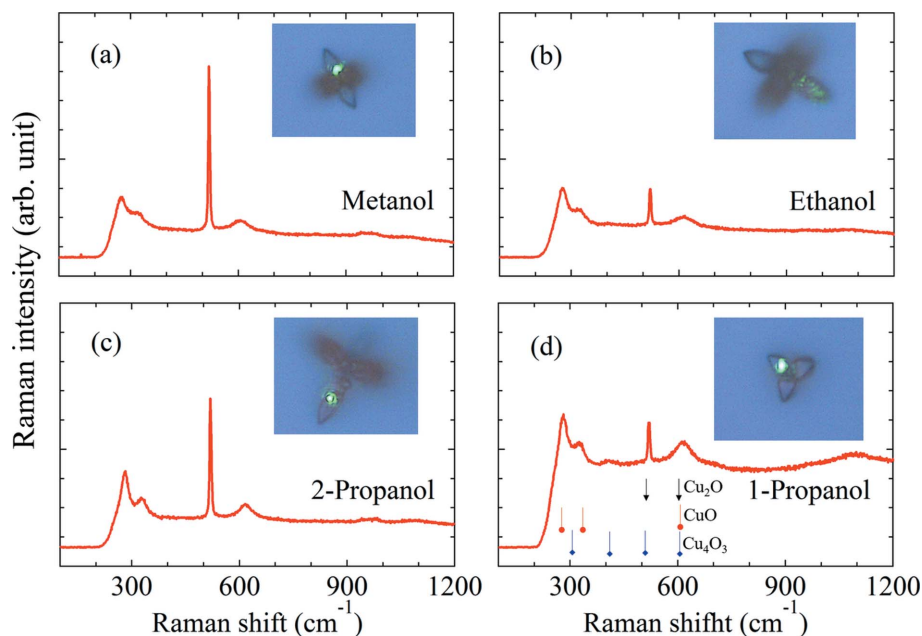


Figure 8
Average blade length as a function of linear alcohol chain number. This graph is a summary of the results shown in Fig. 7. The error bars constitute 1σ , which are determined from the results in Fig. 7.


Figure 9

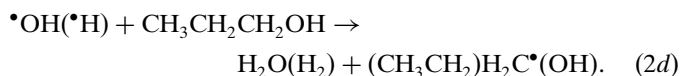
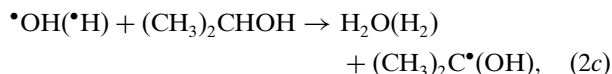
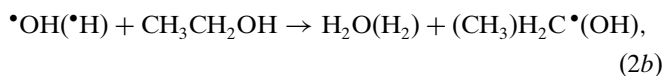
Micro-laser Raman spectra of the particles synthesized by the X-ray irradiation of aqueous $\text{Cu}(\text{COOCH}_3)_2$ solution with the additive (a) methanol (R-1), (b) ethanol (R-2), (c) 2-propanol (R-2') and (d) 1-propanol (R-3). The insets are optical micrographs of the particles; the position of the green light indicates the measurement position of the excitation laser (wavelength 532 nm).

complex inter-relationship between different cupric materials and radical reactions.

Accordingly, we expose the aqueous solution with additive alcohols to X-ray radiation. As is well known, metallic particles are produced by a redox reaction within the solution. The X-ray or γ -ray irradiation technique enables us to easily induce chemical reactions to obtain novel metallic particles, as the X-ray or γ -ray irradiation from synchrotron radiation provides hydrogen and hydroxyl radicals in the following manner (Weiss, 1944, 1946; Miller, 1950; Samuel & Magee, 1953; Henglein, 2000; Johnsen *et al.*, 1969; Buxton *et al.*, 1988):



We also need to consider the additive alcohols. According to Henglein (2000) and Ervens *et al.* (2003), the effects can be described as follows,



Considering the reaction kinetics for a radical scavenger, the k_{H} values of methanol (R-1), ethanol (R-2), 1-propanol (R-3) and 2-propanol (R-2') to $\bullet\text{OH}$ are deduced to be 3.3×10^8 , 1.05×10^9 , 1.6×10^9 and $2.1 \times 10^9 \text{ L mol}^{-1} \text{ s}^{-1}$, respectively

(Buxton *et al.*, 1988; Ervens *et al.*, 2003). Here, k_{H} is the effective reaction rate constant. The value of k_{H} for the $\bullet\text{OH}$ reaction of methanol is the smallest among the values described here. The blade length in the case of ethanol is larger than that for 1-propanol, while k_{H} for ethanol is smaller than that for 1-propanol. This indicates that k_{H} is not an adequate parameter to describe the reaction, and other physical or chemical parameters need to be considered. Here, we check the activation energy associated with the Arrhenius equation. Following the study considering the correlation between activation energy E_{A} and bond dissociation energy, E_{A} values of methanol, ethanol, 1-propanol and 2-propanol are given as 4.8 , 10 ± 3 , 8 ± 6 and 5 kJ mol^{-1} , respectively.¹ The activation energy of 2-propanol is smaller than for the others and the corresponding k_{H} is the largest. This indicates that the strongest X-ray radiolysis-induced chemical reaction is

expected for the additive 2-propanol. From Ervens *et al.* (2003), k_{H} of acetone and acetic acid are 3.5×10^7 and $5.7 \times 10^6 \text{ L mol}^{-1} \text{ s}^{-1}$, respectively. They are much smaller than the values for methanol, ethanol, 1-propanol and 2-propanol. Here, it turns out that the reaction with acetone and acetic acid can be excluded. This is in good agreement with the probability densities of the particle length as shown in Fig. 8.

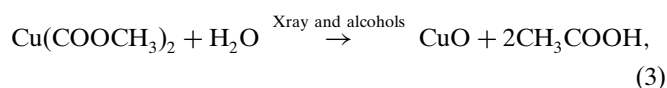
Next, we show micro-laser Raman spectra in order to determine the composition of the cupric oxide particles as shown in Fig. 9. The optical photographs shown in the insets in Fig. 9 represent the positions where the micro-Raman spectra are measured. The bright green position corresponds to the laser spot. A peak at 520 cm^{-1} is deduced to be the Raman signal from the Si substrate. There are three cupric oxide candidates: CuO , Cu_2O and Cu_4O_3 . Peaks at 283 , 333 and 622 cm^{-1} are deduced to be Raman signals from the A_{g} (283.8 cm^{-1}) and B_{g} (333.5 and 622.5 cm^{-1}) modes of cupric oxide CuO (Zhang *et al.*, 2014; Volanti *et al.*, 2008; Yamaguchi *et al.*, 2016b, 2017; Long *et al.*, 2009). Here, according to Debbichi *et al.* (2012), A_{g} and B_{g} denote the Raman modes only with the oxygen atom displacement along the b direction and perpendicular to the b axis, respectively.

We also analyze the crystal structure of the particles synthesized from the $[\text{Cu}(\text{CH}_3\text{COO})_2]$ solution with the additive alcohols [methanol, ethanol # (1/200), ethanol # (1/2000), 1-propanol and 2-propanol] by X-ray diffraction (XRD) as shown in Fig. 10. Here, ethanol # (1/200) and # (1/2000) mean that the additive ethanol ratios with respect to

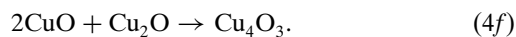
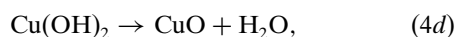
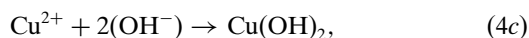
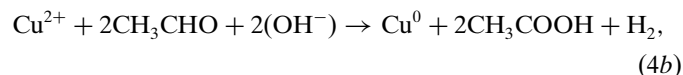
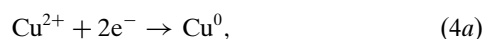
¹ Although the rate constant for the reaction of OH with 1-butanol has not been reported, the constant with respect to *tert*-butanol has been investigated. According to Ervens *et al.* (2003), $k_{\text{H}} = 4.8 \times 10^7 \text{ L mol}^{-1} \text{ s}^{-1}$ and $E_{\text{A}} = 10 \pm 3 \text{ kJ mol}^{-1}$.

the $[\text{Cu}(\text{CH}_3\text{COO})_2]$ solution are 1/200 and 1/2000, respectively. In two cases, we siphoned off 200 μL of the stock solution, 0.37 M $\text{Cu}(\text{COOCH}_3)_2$, into a microtube, and added 1 and 0.1 μL of ethanol, respectively. CuO is indeed synthesized by X-ray radiolysis in all cases. The particles synthesized with methanol and 2-propanol are formed to contain primarily Cu, while those particles obtained with ethanol and 1-propanol are composed of mostly CuO. This result indicates that the reaction is dependent on the linear alcohol chain structure. The formation of Cu_2O is also confirmed in the particles synthesized with methanol and ethanol # (1/200). For Cu_4O_3 , the (312) peak at $2\theta = 52.87^\circ$ (PDF card: number 00-0033-0480) has a substantial overlap with the (020) CuO peak. Considering the micro-Raman spectroscopy and XRD measurement results, it is undeniable that the synthesized particles contain Cu_4O_3 . Consequently, no single-phase Cu, Cu_2O , CuO or Cu_4O_3 particles are obtained but a mixture of these particles are formed with some carbonaceous particles through X-ray radiolysis. An amorphous state is also considered to be formed as part of the synthesized particles.

As investigated in the above studies, we propose the following possible reaction mechanism,



through the following reactions



X-ray radiolysis of the $\text{Cu}(\text{COOCH}_3)_2$ solution in the presence of methanol, ethanol, 2-propanol or 1-propanol results in caltrop cupric oxide particles through the nucleation (Buxton *et al.*, 1988; Ervens *et al.*, 2003), growth and aggregate process (LaMer & Dinegar, 1950; LaMer, 1952; Matijevic, 1994; Privman *et al.*, 1999). In these previous studies, methanol, ethanol or 2-propanol has been introduced as a $\bullet\text{OH}$ scavenger to avoid oxidation of the metal particles. In our study, we find that 1-propanol can also contribute to the synthesis of particles in X-ray radiolysis using white X-rays of ~ 12 keV, but alcohols whose chain lengths are longer than four lose the capability to synthesize the particles. The generation process of highly active radicals which can reduce the metallic ions can be controlled by X-ray energy, flux and the chain length of the additive alcohol.

Finally, we investigated the pH dependence of X-ray radiolysis with ethanol. We cannot obtain particles immobilized on the substrates except for the cases of pH = 3, 6 and 7. Therefore, we describe only the experimental results for the particles obtained in the cases of pH = 3, 6 and 7. Fig. 11 shows SEM images of the particles synthesized for the respective

Table 3

Summary of EDX analyses of the particles synthesized in the solution adjusted at pH = 3, 6 and 7.

	C (at%)	O (at%)	Si (at%)	Cu (at%)	Cu:O
pH 3	45.05	–	51.73	3.23	–
pH 6	54.08	14.35	2.70	28.87	2.01
pH 7	62.38	9.06	9.78	18.79	2.07

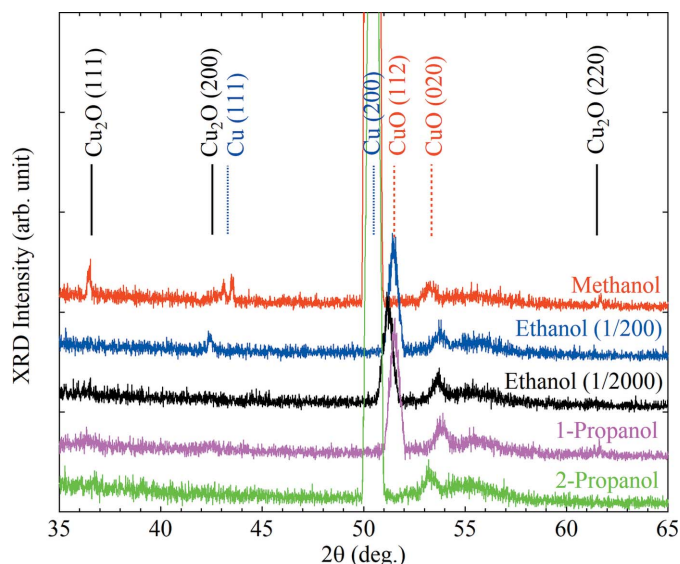


Figure 10

XRD patterns of the cupric particles synthesized in the 5 min X-ray irradiation of the solutions with methanol, ethanol (1/200), ethanol (1/2000), 1-propanol and 2-propanol.

conditions. In the case of pH = 3, monodisperse cubic particles are immobilized onto the silicon substrate after washing. In contrast, round-shaped particles are obtained in the case of pH = 7. The corresponding EDX analyses are summarized in Table 3. It should be noted that cubic particles synthesized in the case of pH = 3 do not contain oxygen, while the other particles synthesized at pH = 6 and 7 include oxygen. Judging from the SEM observation and EDX analysis, the particles obtained at pH = 3 are considered to be pure Cu cubic particles with (100) faces (Mott *et al.*, 2007). The composition ratios of copper and oxygen are almost the same for both cases of pH = 6 and 7. Here, the EDX splitting peak around 0.9–1.0 keV needs to be considered as it is a signature of the presence of Cu as described above. By comparing each spectrum in Fig. 11(d), the EDX spectrum is not split for pH = 3, while the other spectra are split or composed of several peaks. The difference is attributed to the selection rule, splitting degeneracy and electron state modulation by oxidation (Johnsen *et al.*, 1969). Besides, the Raman spectra of both particles obtained at pH = 6 and 7 in Fig. 12 are similar. Hence, we conclude that the particles synthesized at pH = 6 and 7 are similar in composition even though the shapes are different. The rather smooth surface of the spherical polycrystals may be due to the dependence of the pH on the kinetic growth speed of the crystal faces due to the differences in surface energy, resulting in differences in capping agent adsorption. It is very important to note that the final size and shape of the particles

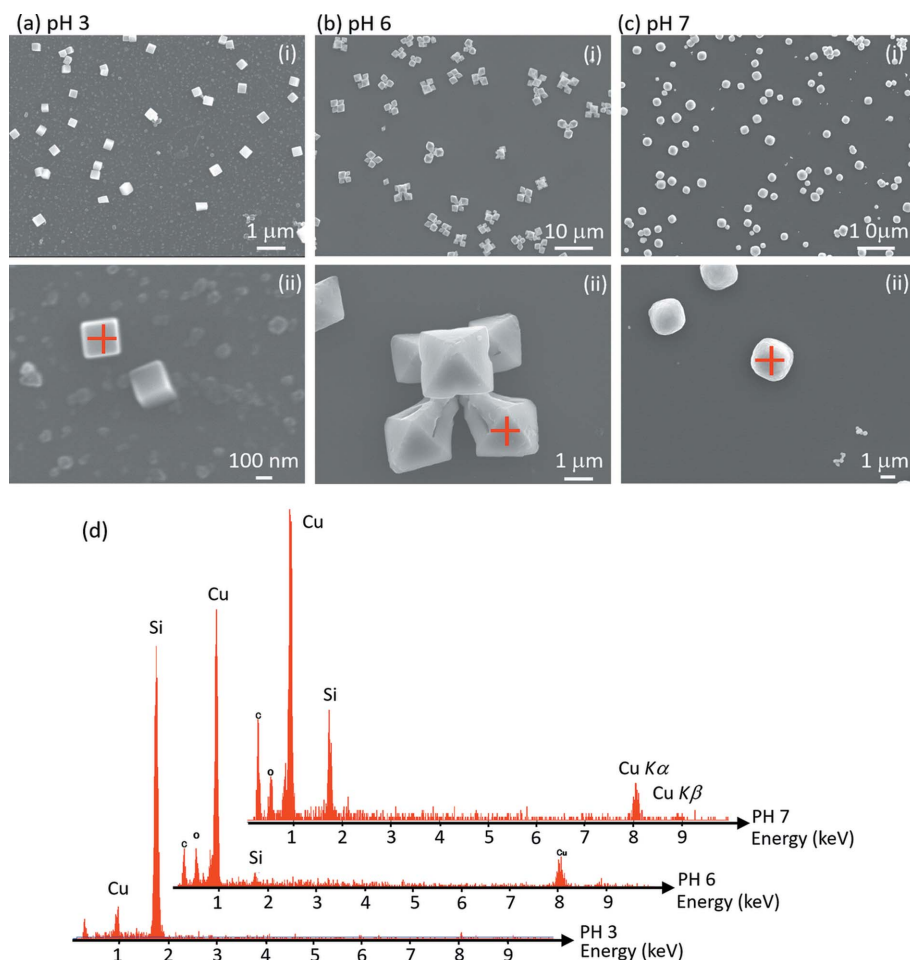


Figure 11
SEM images of cupric particles synthesized by X-ray radiolysis at pH = 3 (a), 6 (b) and 7 (c). High-resolution SEM images are shown in the lower images. (d) Comparison of EDX spectra obtained from the red-cross points shown in (a), (b) and (c).

is not solely dependent on the seed shape but also on the total growth time of the particle, as previously reported (Dey, 2005, 2011; Bárta *et al.*, 2010; Yamaguchi *et al.*, 2015, 2016a,b, 2017; Bharti *et al.*, 2016) as well as solution pH. Thus, X-ray radiolysis, pH, X-ray radiation time and additive alcohol are key parameters to achieve precise control of the particle formation.

Our investigation demonstrates the novel synthesis of caltrop cupric oxide particles deposited onto a Si substrate under the irradiation of synchrotron radiation X-rays. This work also leads to additive alcohol chain number dependence of synthesized particles, helping to understand the process and mechanism of synthesis of the particles. The size, shape and stability of the cupric particles are found to be controlled by the pH, X-ray irradiation time and additive alcohol type. This method allows us to achieve fast synthesis of nano/microparticles and clusters in solution at room temperature. Therefore, our preparation method is applicable to engineering processes such as additive manufacturing processes and three-dimensional printing (Saile *et al.*, 2009; Sachs *et al.*, 1992; Gibson *et al.*, 2015).

4. Conclusion

Caltrop cupric oxide particles have been prepared successfully in cupric acetate $\text{Cu}(\text{COOCH}_3)_2$ solution with additive alcohol using X-ray radiolysis. The blade length of the synthesized particles is found to be dependent on the chain length of the additive alkyl alcohol. Here, there is an upper limit of the chain length of the alcohol to synthesize the particles in aqueous solution of three. This suggests that competition between the generation of hot radicals, which can reduce the metallic ions, and the scavenging activity of $\cdot\text{OH}$ radicals occurred during the synthesis. In other words, the nucleation stage and growth process of particles in the X-ray radiolysis can be controlled by X-ray energy, flux and chain length of the additive alkyl alcohol. The chain length dependence of the synthesized particles provides a glimpse of the X-ray radiolysis.

Direct X-ray irradiation using a synchrotron radiation source can shed light on exploring novel physical and chemical mechanisms of liquid/solid interlayer reaction process from a liquid phase. Our deposition process can be utilized as a means of fabricating higher-order nano/microstructure consisting of metallic particles and metal oxide particles onto a lab-on-a-chip and micro-Total-Analysis-System (μTAS)

device for chemical, environmental and diagnosing analyses. The development of this method enables integrating three-dimensional printing and additive manufacturing.

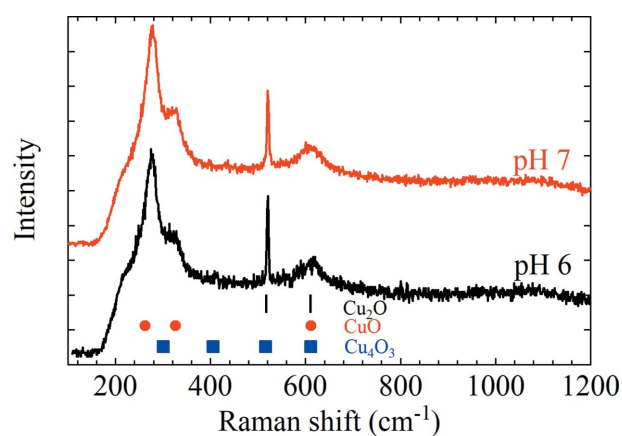


Figure 12
Micro-laser Raman spectra of the particles synthesized by the X-ray irradiation of aqueous $\text{Cu}(\text{COOCH}_3)_2$ solution at pH = 6 and 7.

Acknowledgements

We are grateful to Dr Atsushi Yamaguchi of Hyogo Prefectural Institute of Technology for SEM and EDX measurement support. We appreciate Dr Saiki and Dr Takizawa of Hyogo Prefectural Institute of Technology for fruitful discussions. We thank Mitsutoyo Association for Science and Technology.

Funding information

This research and development work was supported in part by MIC/SCOPE grant No. 152107006 and by JSPS Grants-in-Aid for Scientific Research B (No. 17H02755). These experiments were conducted at the BL8S2 of Aichi Synchrotron Radiation Center, Aichi Science and Technology Foundation, Aichi, Japan (Proposal No.2018a0016 & No.2017a0049) with the financial support of Synchrotron Radiation Research Center, Nagoya University. EJ is supported by Jeol UK and KE is supported by JST CREST (No. JPMJCR17J5). This work is partially supported by JSPS-EPSCRC Core-to-Core Programme (EP/M02458X/1)

References

Albrecht, M. G. & Creighton, J. A. (1977). *J. Am. Chem. Soc.* **99**, 5215–5217.

Athawale, A. A., Katre, P. P., Kumar, M. & Majumdar, M. B. (2005). *Mater. Chem. Phys.* **91**, 507–512.

Bae, C. H., Nam, S. H. & Park, S. M. (2002). *Appl. Surf. Sci.* **197–198**, 628–634.

Bang, J. H. & Suslick, K. S. (2010). *Adv. Mater.* **22**, 1039–1059.

Bárta, J., Pospíšil, M. & Čuba, V. (2010). *J. Radioanal. Nucl. Chem.* **286**, 611–618.

Barton, A. F. M. (1984). *Alcohols with Water (Solubility Data Series)*, Vol. 15, 1st ed. Pergamon Press.

Bharti, A., Bhardwaj, R., Agrawal, A. K., Goyal, N. & Gautam, S. (2016). *Sci. Rep.* **6**, 22394.

Borse, P. H., Yi, J. M., Je, J. H., Choi, S. D., Hwu, Y., Ruterana, P. & Nouet, G. (2004a). *Nanotechnology*, **15**, S389–S392.

Borse, P. H., Yi, J. M., Je, J. H., Tsai, W. L. & Hwu, Y. (2004b). *J. Appl. Phys.* **95**, 1166–1170.

Brookshier, M. A., Chusuei, C. C. & Goodman, D. W. (1999). *Langmuir*, **15**, 2043–2046.

Buxton, G. V., Greenstock, C. L., Helman, W. P. & Ross, A. B. (1988). *J. Phys. Chem. Ref. Data*, **17**, 513–886.

Caruso, R. A., Ashokkumar, M. & Grieser, F. (2002). *Langmuir*, **18**, 7831–7836.

Clay, R. T. & Cohen, R. E. (1998). *New J. Chem.* **22**, 745.

Cushing, V. L., Kolesnichenko, V. L. & O'Connor, S. J. (2004). *Chem. Rev.* **104**, 3893–3946.

Dar, M. A., Ahsanulhaq, Q., Kim, Y. S., Sohn, J. M., Kim, W. B. & Shin, H. S. (2009). *Appl. Surf. Sci.* **255**, 6279–6284.

Debbichi, L., Marco de Lucas, M. C., Pierson, J. F. & Krüger, P. (2012). *J. Phys. Chem. C*, **116**, 10232–10237.

Dey, G. R. (2005). *Radiat. Phys. Chem.* **74**, 172–184.

Dey, G. R. (2011). *Radiat. Phys. Chem.* **80**, 1216–1221.

Ervens, B., Gligorovski, S. & Herrmann, H. (2003). *Phys. Chem. Chem. Phys.* **5**, 1811–1824.

Fievet, F., Lagier, J., Blin, B., Beaudoin, B. & Figlarz, M. (1989). *Solid State Ionics*, **32–33**, 198–205.

Figlarz, M., Fievet, F. & Lagier, J. P. (1985). French Patent 8 221 483.

Fleisch, T. H. & Mains, G. J. (1982). *Appl. Surf. Sci.* **10**, 51–62.

Frens, G. (1972). *Colloid Polym. Sci.* **250**, 736–741.

Frens, G. (1973). *Nature*, **241**, 20–22.

Gedanken, A. (2004). *Ultrason. Sonochem.* **11**, 47–55.

Gibson, I., Rosen, D. & Stucker, B. (2015). *Additive Manufacturing Technologies: 3D Printing, Rapid Prototyping and Direct Digital Manufacturing*, 2nd ed. Springer.

Goldstein, J. L., Newbury, D., Joy, D., Lyman, C., Echlin, P., Lifshim, E., Sawyer, L. & Michael, J. (2003). *Scanning Electron Microscopy and X-ray Microanalysis*, 3rd ed, New York: Springer Science and Business Media.

Hara, R., Fukuoka, T., Takahashi, R., Utsumi, Y. & Yamaguchi, A. (2015). *RSC Adv.* **5**, 1378–1384.

Hashimoto, S., Uwada, T., Hagiri, M. & Shiraishi, R. (2011). *J. Phys. Chem. C*, **115**, 4986–4993.

Haynes, C. L., McFarland, A. D. & Van Duyne, R. P. (2005). *Anal. Chem.* **77**, 338A–346A.

Henglein, A. (2000). *J. Phys. Chem. B*, **104**, 1206–1211.

Izaki, M., Shinagawa, T., Mizuno, K., Ida, Y., Inaba, M. & Tasaka, A. (2007). *J. Phys. D Appl. Phys.* **40**, 3326–3329.

Johnsen, R. H., Barker, N. T. & Burgin, M. (1969). *J. Phys. Chem.* **73**, 3204–3208.

Kim, J. Y., Park, J. C., Kang, H., Song, H. & Park, K. H. (2010). *Chem. Commun.* **46**, 439–441.

Kreibig, U. & Vollmer, M. (1995). *Optical Properties of Metal Clusters*, Springer Series in Material Science, Vol. 25. Berlin: Springer.

Kvítek, L., Panáček, A., Soukupová, J., Kolář, M., Večeřová, R., Prucek, R., Holecová, M. & Zbořil, R. (2008). *J. Phys. Chem. C*, **112**, 5825–5834.

LaMer, V. K. (1952). *Ind. Eng. Chem.* **44**, 1270–1277.

LaMer, V. K. & Dinegar, R. H. (1950). *J. Am. Chem. Soc.* **72**, 4847–4854.

Lee, H. J., Je, J. H., Hwu, Y. & Tsai, W. L. (2003). *Nucl. Instrum. Methods Phys. Res. B*, **199**, 342–347.

Le Ru, E. C. & Etchegoin, P. G. (2009). *Principles of Surface-Enhanced Raman Spectroscopy and Related Plasmonic Effects*. Amsterdam: Elsevier.

Lisiecki, I. & Pileni, M. P. (1993). *J. Am. Chem. Soc.* **115**, 3887–3896.

Long, J., Dong, J., Wang, X., Ding, Z., Zhang, Z., Wu, L., Li, Z. & Fu, X. (2009). *J. Colloid Interface Sci.* **333**, 791–799.

Lu, X., Rycenga, M., Skrabalak, S. E., Wiley, B. & Xia, Y. (2009). *Annu. Rev. Phys. Chem.* **60**, 167–192.

Ma, Q., Moldovan, N., Mancini, D. C. & Rosenberg, R. A. (2000). *Appl. Phys. Lett.* **76**, 2014–2016.

Matijevic, E. (1994). *Langmuir*, **10**, 8–16.

Miller, N. (1950). *J. Chem. Phys.* **18**, 79–87.

Mori, Y., Kitamoto, N., Matsuda, S. & Tsuchiya, K. (2004). *Asian Pacific Confederation of Chemical Engineers Congress Program and Abstracts*, Volume 2004, p. 145, Session ID 3D-04 (<http://doi.org/10.11491/apcche.2004.0.145.0>).

Mott, D., Galkowski, J., Wang, L., Luo, J. & Zhong, C. J. (2007). *Langmuir*, **23**, 5740–5745.

Nagata, Y., Watanabe, Y., Fujita, S., Dohmaru, T. & Taniguchi, S. (1992). *J. Chem. Soc. Chem. Commun.* p. 1620.

Nie, S. & Emory, S. R. (1997). *Science*, **275**, 1102–1106.

Okitsu, K., Yue, A., Tanabe, S., Matsumoto, H. & Yobiko, Y. (2001). *Langmuir*, **17**, 7717–7720.

Park, J. C., Kim, A. Y., Kim, J. Y., Park, S., Park, K. H. & Song, H. (2012). *Chem. Commun.* **48**, 8484–8486.

Poizot, P., Laruelle, S., Grugeon, S., Dupont, L. & Tarascon, J. M. (2000). *Nature*, **407**, 496–499.

Privman, V., Goia, D. V., Park, J. & Matijević, E. (1999). *J. Colloid Interface Sci.* **213**, 36–45.

Radi, A., Pradhan, D., Sohn, Y. & Leung, K. T. (2010). *ACS Nano*, **4**, 1553–1560.

Remita, S., Fontaine, P., Lacaze, E., Borensztein, Y., Sellame, H., Farha, R., Rochas, C. & Goldmann, M. (2007). *Nucl. Instrum. Methods Phys. Res. B*, **263**, 436–440.

Remita, S., Fontaine, P., Rochas, C., Muller, F. & Goldmann, M. (2005). *Eur. Phys. J. D*, **34**, 231–233.

- Rosenberg, R. A. (1998). *J. Vac. Sci. Technol. B*, **16**, 3535.
- Sachs, E., Cima, M., Williams, P., Branzazio, D. & Cornie, J. (1992). *J. Eng. Ind.* **114**, 481–488.
- Saile, V., Wallradbe, U., Tabata, O. & Korvink, J. G. (2009). *Advanced Micro and Nanosystems*, Vol. 7, *LIGA and its Applications*. Weinheim: Wiley-VCH.
- Samuel, A. H. & Magee, J. L. (1953). *J. Chem. Phys.* **21**, 1080–1087.
- Shao, W., Pattanaik, G. & Zangari, G. (2007). *J. Electrochem. Soc.* **154**, D339–D345.
- Su, D., Xie, X., Dou, S. & Wang, G. (2014). *Sci. Rep.* **4**, 5753.
- Suslick, K. S., Choe, S., Cichowlas, A. A. & Grinstaff, M. W. (1991). *Nature*, **353**, 414–416.
- Takami, A., Kurita, H. & Koda, S. (1999). *J. Phys. Chem. B*, **103**, 1226–1232.
- Tamaki, J., Shimano, K., Yamada, Y., Yamamoto, Y., Miura, N. & Yamazoe, N. (1998). *Sens. Actuators B Chem.* **49**, 121–125.
- Tsuji, M., Hashimoto, M., Nishizawa, Y., Kubokawa, M. & Tsuji, T. (2005). *Chem. Eur. J.* **11**, 440–452.
- Tu, W. & Liu, H. (2000). *J. Mater. Chem.* **10**, 2207–2211.
- Volanti, D. P., Keyson, D., Cavalcante, L. S., Simões, A. Z., Joya, M. R., Longo, E., Varela, J. A., Pizani, P. S. & Souza, A. G. (2008). *J. Alloys Compd.* **459**, 537–542.
- Wagner, J. & Köhler, J. M. (2005). *Nano Lett.* **5**, 685–691.
- Weiss, J. (1944). *Nature*, **153**, 748–750.
- Weiss, J. (1946). *Nature*, **157**, 584.
- Wiley, B., Herricks, T., Sun, Y. & Xia, Y. (2004). *Nano Lett.* **4**, 1733–1739.
- Yamaguchi, A., Fukuoka, T., Okada, I., Ishihara, M., Sakurai, I. & Utsumi, Y. (2017). *J. Synchrotron Rad.* **24**, 653–660.
- Yamaguchi, A., Matsumoto, T., Okada, I., Sakurai, I. & Utsumi, Y. (2015). *Mater. Chem. Phys.* **160**, 205–211.
- Yamaguchi, A., Okada, I., Fukuoka, T., Sakurai, I. & Utsumi, Y. (2016a). *Jpn. J. Appl. Phys.* **55**, 055502.
- Yamaguchi, A., Okada, I., Sakurai, I., Fukuoka, T., Ishihara, M. & Utsumi, Y. (2016b). *J. Nanomater.* **2016**, 8584304.
- Yamamoto, T., Wada, Y., Sakata, T., Mori, H., Goto, M., Hibino, S. & Yanagida, S. (2004). *Chem. Lett.* **33**, 158–159.
- Yates, B. W. & Shinozaki, D. M. (1993). *J. Polym. Sci. B Polym. Phys.* **31**, 1779–1784.
- Yeh, M., Yang, Y.-P., Lee, Y., Lee, H., Yeh, Y. & Yeh, C.-S. (1999). *J. Phys. Chem. B*, **103**, 6851–6857.
- Zaman, S., Asif, M. H., Zainelabdin, A., Amin, G., Nur, O. & Willander, M. (2011). *J. Electroanal. Chem.* **662**, 421–425.
- Zaman, S., Zainelabdin, A., Amin, G., Nur, O. & Willander, M. (2012). *J. Phys. Chem. Solids*, **73**, 1320–1325.
- Zhang, J., Liu, J., Peng, Q., Wang, X. & Li, Y. (2006). *Chem. Mater.* **18**, 867–871.
- Zhang, Q., Zhang, K., Xu, D., Yang, G., Huang, H., Nie, F., Liu, C. & Yang, S. (2014). *Prog. Mater. Sci.* **60**, 208–337.
- Zhang, Z., Sun, H., Shao, X., Li, D., Yu, H. & Han, M. (2005). *Adv. Mater.* **17**, 42–47.